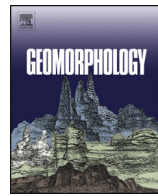




Contents lists available at ScienceDirect



Geomorphology

journal homepage: www.elsevier.com/locate/geomorph

Numerical modeling of the evolution of arcades and rock pillars

Alexander Safonov ^a, Michal Filippi ^{b,*}, David Mašín ^c, Jiří Bruthans ^c^a Skolkovo Institute of Science and Technology, Center for Design, Manufacturing and Materials, Moscow, Russia^b Institute of Geology of the Czech Academy of Sciences, Rozvojová 269, 165 00 Prague 6, Czech Republic^c Faculty of Science, Charles University, Albertov 6, 128 43 Prague 2, Czech Republic

ARTICLE INFO

Article history:

Received 3 March 2020

Received in revised form 14 May 2020

Accepted 15 May 2020

Available online 18 May 2020

Keywords:

Sandstone

Arcades

Pillars

Rock stress

Weathering

ABSTRACT

Arcades, i.e. lenticular and other specifically shaped hollows controlled by discontinuities, have recently been recognized as a weathering form typical for sandstones, weathered quartzites, granites, or tuffs. They are produced by accelerated weathering and erosion in stress shadows related to the redistribution of gravity-induced stress along planar discontinuities in the rock. These forms occur worldwide in various settings (inland humid, arid, and coastal). The origin of arcades has been demonstrated via physical experiments and supported by a relatively simplistic numerical modeling. However, details on their shaping and the evolution of related forms have not been explained. We performed an advanced numerical modeling to produce various shapes of arcades and rock pillars during the erosion of rock masses dissected by discontinuities. We demonstrate that the erosion model, in which erosion takes place when the maximum principal stress is below a certain critical value, can adequately describe the formation of arcades. In the modeling, we set higher critical values for stresses at discontinuities than in a homogeneous material (representing a rock mass) to represent the higher tendency for disintegration of the discontinuity material, which was weakened by the discontinuity formation processes. By applying various discontinuity geometries and values of critical stresses, we were able to reproduce the formation of various arcade shapes and complex-three-dimensional clusters of arcade cavities with rock pillars. Discontinuities and stress-controlled erosion/weathering are the only necessary conditions for arcade formation.

© 2020 Elsevier B.V. All rights reserved.

1. Introduction

1.1. Broader context

The principal idea of negative feedback between stress and erosion as a controlling factor for the origin and evolution of the specific class of natural landforms in interlocked granular rocks was proposed in 2014 (Bruthans et al., 2014). This idea of stress-controlled erosion was then used in the modeling of the retreat of man-made cavities in the ancient city of Petra (Rihosek et al., 2016). The origin of arcades (see below) corresponds well with this idea. Most recently, the principle of interaction among gravity-induced stress, discontinuity, and stress-controlled erosion was demonstrated in small-scale physical modeling of a rock arch to explain the origin of a large group of real natural rock arches (Řihošek et al., 2019). The afore-mentioned studies and also Moore et al. (2020) showed the indisputable usefulness of the numerical modeling of stress distribution and erosion in understanding the origin of sandstone weathering forms. However, this modeling approach is still in its infancy and much remains unexplained.

Although newly characterized, arcades seem to be a ubiquitous phenomenon in many sandstone landscapes around the world (see figs. 6–9, 23, and 25 in Filippi et al., 2018 and Fig. 1 in this paper). In some areas, arcades are even more common than honeycombs (e.g., Arches and Zion National Parks in Utah, Wadi Rum in Jordan, and Apolena Rock City in the Czech Republic). At many places, arcades and other related stress-controlled forms appear to be essential for shaping of entire sandstone outcrops (e.g., fig. 30 in Filippi et al., 2018 and Fig. 1B, E in this paper). Therefore, we address the process of arcade formation in more detail in this paper.

1.2. Arcade types and related complex weathering forms: explaining their origin

Arcades have been segregated from large groups of cavernous weathering forms (Filippi et al., 2018). They have been shown to differ from honeycombs/tafoni and some other types of cavities and rock shelters in their clear association with planar discontinuities, their geometry, and their origin. They are a product of the redistribution of gravity-induced stress along planar discontinuities originated due to accelerated weathering and erosion in stress shadows, i.e., zones of low stress (Bruthans et al., 2014). Several arcade types can be distinguished based on their various shape complexity. Generally, arcades form

* Corresponding author.

E-mail address: filippi@gli.cas.cz (M. Filippi).

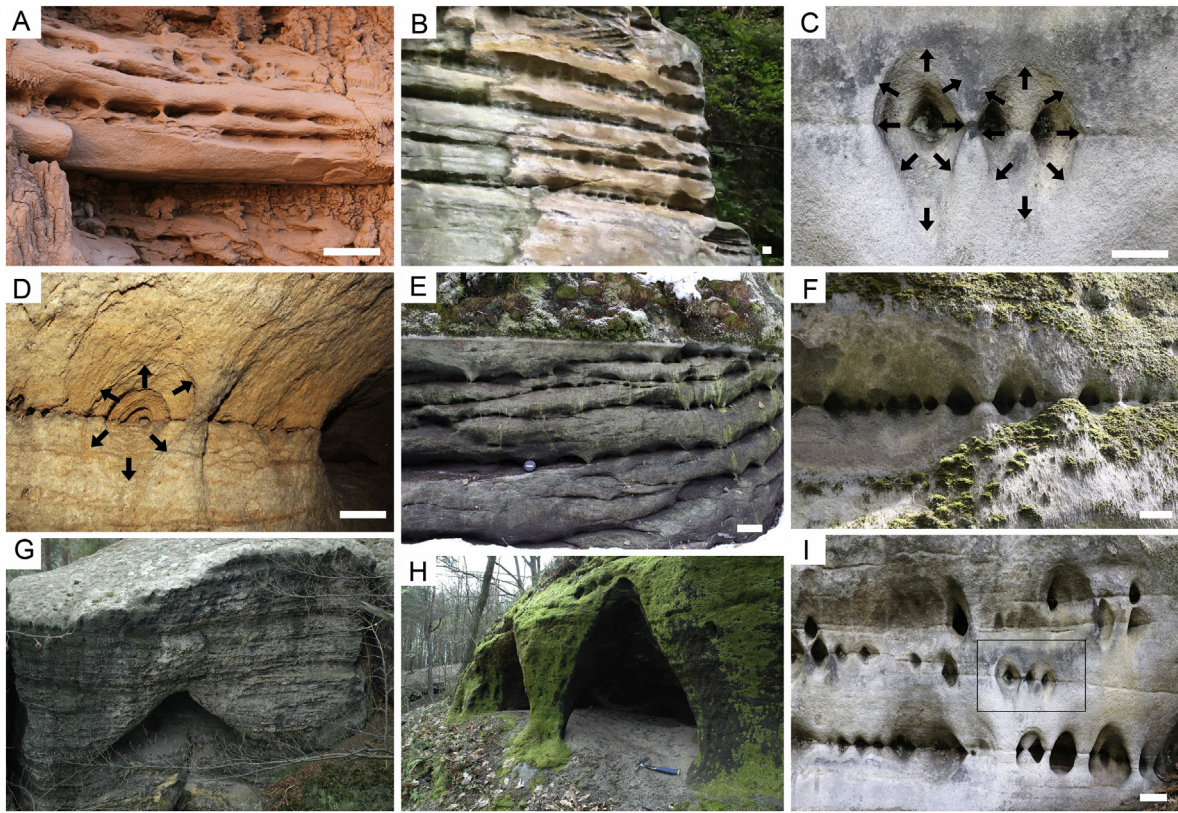


Fig. 1. Examples of various arcades and arcade-related cavities (a 10 cm scale bar is shown where necessary). A: Thin grooves with rather low and roughly equal arcades on the bottom step of an intermittent surface stream, Goblin Monument, USA. B: Thin grooves with rather low and roughly equal arcades on a cliff face, Apolena Rock City, CZ. C: Merging of stress shadows of four small rhombic arcades leads to formation of two larger cavities (follow the lines indicated as black arrows) of higher order (a thumbnail from photo I), Apolena Rock City, CZ. D: Enlargement (growth) of a vaulted arcade into a larger cavity of higher order, underground environment in the Adršpach-Teplice Cliffs monument, CZ. E: Asymmetrical arcades on a cliff face periodically flooded by a lake for several decades, Adršpach-Teplice Cliffs monument, CZ. F: Irregular rhombic arcades; note the symmetrical lenticular area free of mosses, i.e., area of weakened sandstone, most probably defining the extent of stress shadows, Apolena Rock City, CZ. G: A large sole symmetrical rhombic arcade-derived cavity, Kobylka Gorge, Mšeno area, CZ. H: Two large symmetrical rhombic arcade-derived cavities separated by a pillar, northern slopes of Šibeník Hill, Dubá area, CZ (photos G–H by J. Adamovič). I: Mostly rhombic arcades in various stages of their development; chains of separate cavities, incipient arcades of a higher order, and a complex 3D structure with rock pillars, Apolena Rock City, CZ.

roughly regular pits and cavities, either symmetrical along planar discontinuities or asymmetrical, developed partly or fully on one side only. Adjacent pits are separated by inconspicuous abutments to distinctive hourglass-shaped rock pillars. Arcade pits are mostly clustered into linearly-arranged “trains” consisting of several pits.

Numerical modeling by Filippi et al. (2018) supported the existence of symmetrical (lenticular) arcade cavities via 2D models. Stress distribution around a narrow incision was modeled, showing that areas of reduced stress (stress shadows) are located below and above the incision. Simultaneously, more stressed zones develop on both margins of the incision. This stress distribution results in a dominant erosion from the zones of stress shadows, giving rise to symmetrical arcades. The use of bigger chained lenticular “voids” instead of a narrow incision led to the extension of stress shadows along the vertical axis of each void, which explains the origin of rhombic (i.e., rhomb- or diamond-shaped) arcades. These rhombic shapes can be considered the ultimate product of the process (cf. fig. 15a with fig. 14c in Filippi et al., 2018). The evolution of symmetrical arcades/voids was also predicted using a 2D model of the stress-controlled erosion (Supplementary video 1 in Filippi et al., 2018). Nevertheless, advanced modeling of arcade evolution was needed because the formation of more complex three-dimensional (3D) arcade structures with rock pillars and the evolution of asymmetrical arcades could not be explained by a simplified 2D approach (an arcade is an inherently 3D phenomenon, which can only schematically be demonstrated using 2D models).

Modeling of the evolution of asymmetrical arcades is a considerable challenge, because a large stress shadow develops beneath the flat

bottom of the half-lenticular void in this case, as is obvious in fig. 15c, d in Filippi et al. (2018). This stress shadow should determine where the erosion takes place. However, as has been documented in natural outcrops and observed through physical in situ modeling, asymmetrical arcades are formed and persist. Filippi et al. (2018) explained this dis-harmony between the model and natural observations by induration along some discontinuities, caused, e.g., by tectonic shear (locking or cementing grains), precipitation of iron oxyhydroxides, or by the origin of more complex case hardening crusts on bedding planes.

1.3. Justification of purpose

As stated above, the existence of the most elementary symmetrical arcades has been satisfactorily explained through numerical modeling of stress distribution using the PLAXIS 3D finite-element software. Spontaneous formation of a sole arcade pit was modeled using the Tochnog Professional geotechnical software (Filippi et al., 2018). However, both these approaches were based on predefined discontinuities formed by narrow empty voids (artificially cut incisions, which were used in the physical modeling). The initial shape of the empty void controlled the final horizontal extent of the resulting arcade to a significant degree. In nature, on the contrary, the discontinuity causing the development of symmetrical arcades is generally formed by a thin, easily erodible zone weakened by discontinuity formation processes. This zone is usually characterized by elevated moisture, higher porosity, etc. To capture these natural processes, the model must be capable of capturing the gradual erosion of the discontinuity material and not

just the rock mass in its vicinity. Besides, the existence of asymmetrical arcades or even the formation of sets of arcades and complex arcade clusters with rock pillars have remained unsubstantiated by the numerical modeling so far.

Therefore, in this study, we apply advanced numerical modeling to better explain the existence and, in particular, the formation/evolution of the above-mentioned forms. To achieve this goal, we use the modeling of material properties degradation during natural erosion, using evolutionary algorithms with stress/strain-dependent constitutive relationships (Ostanin et al., 2017; Safonov, 2018, 2019). In contrast with the previous numerical modeling technique, which sets the initial shape of the eroded zone in a mechanically homogeneous rock environment, the approach proposed in this paper allows to model the erosion directly of both the discontinuity and the surrounding rock masses, which may have different properties on both sides of the discontinuity.

2. Methods

2.1. Modeling approach

Each numerical model for the modeling of natural erosion is divided into finite elements. For each finite element i , we assigned material properties depending on the type of material and its erosion state. To describe the erosion of material, for each finite element we introduce the dimensionless artificial density ρ , equal to $\rho_{max} = 1$ for non-eroded material and $\rho_{min} = 0.0001$ for completely eroded material. For each finite element, we assign a critical value, σ_c , to the maximum principal stresses σ_{max} , such that erosion takes place when the maximum principal stress is less than σ_c . The stiffness of the eroded material of a finite element is decreased by the factor of 10,000. Erosion of material in a finite element may only take place when there is another eroded finite element with its center located within the R [mm] distance from the given one, i.e., when there are adjacent eroded elements, which means that the given element is located at the erosion propagation front, Γ . Here we build an iteration algorithm where at each iteration step n for elements located at the erosion front the erosion criterion is checked, i.e., the maximum principal stresses σ_{max} should be less than σ_c . If this criterion is met for such surface elements, then the rigidity of material in this finite element is decreased by the factor of 10,000. Therefore, the iterative algorithm of erosion modeling that determines the values of artificial density for each finite element at each iteration step can be expressed as follows:

$$\rho_i^{n+1} = \begin{cases} \rho_i^n & \text{if } \sigma_{max} \geq \sigma_c \text{ OR } i \notin \Gamma \\ \rho_{min} & \text{if } \sigma_{max} < \sigma_c \text{ AND } i \in \Gamma \end{cases}$$

where i is the finite element, n is the iteration step. The initial distribution of artificial density for non-eroded finite element model is assigned at $n = 1$.

It is to be pointed out that the experimental results (for example, Rihosek et al., 2016) indicate the effect of time in the erosion process (a stress increase results in a decrease in erosion rate) in natural sandstones. In this work, we adopt simpler material modeling concept, observed experimentally on locked sand (Bruthans et al., 2014), where erosion takes place once the stress becomes as low as the critical value. We consider it sufficient to reproduce qualitatively the phenomena observed in nature, while the effect of time will be subject to future research.

Furthermore, we used the filtration method to deal with the possible artifacts of numerical modeling, such as checkerboard instabilities and unnaturally thin structures (Sigmund and Petersson, 1998). We introduce the mean density $\bar{\rho}$ as follows (Klarbring and Torstenfelt, 2010):

$$\bar{\rho}_j = \sum_{i=1}^M \Psi_{ji} \rho_i, \quad j = 1, \dots, M$$

where

$$\Psi_{ij} = \frac{\psi_{ij}}{\sum_{k=1}^M \psi_{ik}}, \quad \psi_{ij} = \max(0, 1 - \frac{|\mathbf{e}_i - \mathbf{e}_j|}{R}),$$

where \mathbf{e}_i shows the position of the element i center, M is the total number of finite elements. Thereby, we force the erosion of the material in finite element j when $\bar{\rho}_j < 0.677$.

2.2. Software used

For numerical modeling of the erosion process, we used the ABAQUS finite-element software suite (version 6.14) (Abaqus Analysis User Manual, 2014). Abaqus allows a researcher to get realistic solutions for nonlinear mechanical problems quickly. Besides, its user subroutines mechanism makes it possible to locally change the mechanical properties and loads distribution during the computation. In this study we used the following user subroutines: USDFLD, URDFIL, DLOAD, and UEXTERNALDB. We used USDFLD to consider changes in mechanical properties in finite elements during the erosion process and URDFIL to access the results of the solution of maximum stress distribution. URDFIL was also used to get the coordinates of the integration points of finite elements and form the array containing the list of adjacent elements for each given finite element. We used DLOAD to assign the surface and bulk forces at each iteration step, depending on the advance of the erosion front or on number of the iteration step (arcade evolution modeling). UEXTERNALDB was used to assign algorithm parameters before modeling. We used allocatable arrays to transfer data arrays between user subroutines during computations. The Fortran programming language was used to implement the user subroutines. In all computations discussed here, we used linear hexahedral elements of the C3D8R type. Although we used only uniform meshes of cubic elements with 5 mm edges, the method proposed here can be applied to computations with a nonuniform mesh of finite elements with arbitrary geometry. The construction of the computational model, including the definition of geometry and material properties, mesh generation, imposition of boundary conditions and generation of the input file were made in the Abaqus/CAE. The solution of the problem was obtained in the Abaqus/Standard product and visualization of the computation results employed the Abaqus/Viewer product. We used the Isosurface view cut for visualization of structures obtained during the modeling. Computer files of user subroutines and ABAQUS numerical models for modeling of symmetrical arcades and pillars can be found at the GitHub repository (Safonov, 2020).

2.3. Experimental settings

We consider a model imitating a rock mass containing a horizontal discontinuity to describe the formation of various arcade types. Typical real-world examples of discontinuities in sandstone are unconformities, bedding planes and clinoform surfaces, cross-bedding foresets, joints, faults, weathering zones along mud- or carbonate-rich interbeds, etc. We used two types of non-eroded material for the rock mass: material 1 to model experiments with Střeleč weak sandstone (which has the behavior of locked sand locally – i.e., consolidated non-cemented sand-sized sediment) from a previous study (Filippi et al., 2018) (Figs. 2, 3, and 4) and material 2 to model the evolution of symmetrical arcades developing into a 3D complex structures with pillars (Fig. 5) and formation of asymmetrical arcades (Fig. 6). Materials 1 and 2 are isotropic. We used Material 3 (transversely isotropic material with the axis of isotropy perpendicular to the discontinuity) to model the mechanical behavior of material in the discontinuity region during the evolution of arcades (Fig. 5) and formation of asymmetrical arcades (Fig. 6). The properties of materials used are listed in Table 1. We used Cartesian coordinate system (x, y, z). Table 1 shows the values of elastic moduli E_x, E_y ,

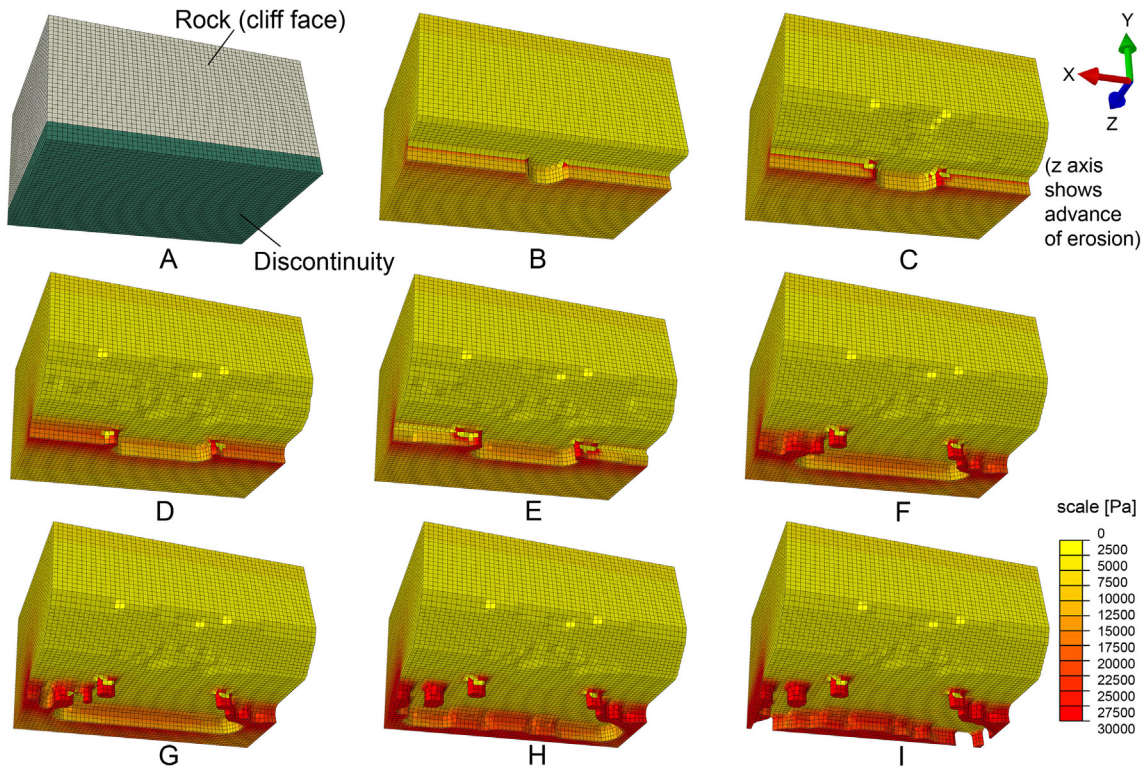


Fig. 2. Modeling of the erosion process with continuous recession of rock. A: Geometrical model including the discontinuity region and regular rock. The dimensions and boundary conditions are described in the Methods section. Panels B–I: Progress of the erosion process in relation to the iteration step, n , during modeling (non-eroded part of the model is shown). The figures show the distribution of the maximum stress. All stresses within the discontinuity region exceeding the disintegration limit of material are shown as disintegration limit stresses. B: Non-eroded model at $n = 1$. Initial eroded zone in the form of an indentation and an additional circular indentation. C: $n = 4$, D: $n = 9$. Advance of the erosion front and expansion of the additional indentation. E: $n = 18$, F: $n = 24$. Formation of the first row of pillars in the corner area. G: $n = 20$, H: $n = 24$, I: $n = 33$. Further advance of the erosion front and formation of secondary pillars.

E_z ; Poisson's ratio ν_{yx} , ν_{xz} , ν_{yz} ; shear modulus G_{yx} , G_{xz} , G_{yz} ; and critical value σ_c .

The dimensions of the model shown in Fig. 2A are as follows: 300 mm length (x), 150 mm height (y), and 200 mm width (z). The discontinuity is adjacent to the lower face of the model. The thicknesses of the discontinuity regions for the models used in the first and second experiments are 20 mm and 10 mm, respectively. Dimensions of the models are chosen based on actual dimensions of experimental specimens used in the study by Filippi et al. (2018). The model is built of uniformly distributed cubic elements with an edge of 5 mm. The following boundary conditions are imposed (Fig. 2A): restricted displacement in the vertical direction (y) at the base of the model, restricted x -displacements at the right and left sides, and restricted z -displacements at the back of the model. No displacement constraints are imposed on the front side of the model. We loaded the model with the gravity force, with gravity acceleration directed vertically opposite to the y axis. Gravity was applied only to finite elements with the non-eroded material. The rock mass density was set equal to 2200 kg/m³. We also loaded the model by applying stress at the top to represent additional overburden. The erosion process was set to initiate at the finite elements in the region adjacent to the free plane.

The model shown in Fig. 5A has a cubic form, with an edge of 200 mm. The size of the model is chosen based on the characteristic dimension (scale bars) of arcades, constituting 100 mm (see Filippi et al., 2018). The discontinuity is adjacent to the central horizontal section. The thickness of the discontinuity is 10 mm. The model is built of uniformly distributed cubic elements, with an edge of 5 mm. The following boundary conditions are imposed (Fig. 5A): restricted vertical (y) displacement at the base of the model, restricted x -displacements at the right and the left sides, and restricted z -displacements at the back of the model. For the model of the asymmetrical arcade formation with

applying lateral stress x -displacement, constraints are applied only at the lower segment of the model (Fig. 5A). No displacement constraints are imposed on the front side of the model. Instead of the gravity force, these models were loaded by applying stress at the top to represent additional overburden of a rock with a height of 5 m. For the model of the asymmetrical arcade formation, in addition to applying lateral stress, we applied additional stress to model the effect of different horizontal stresses within the rock massif developed during the geological rock mass formation processes.

3. Results

3.1. Validation of modeling approach

We focused on the physical modeling experiments presented by Filippi et al. (2018) to validate the modeling approach—experiment C (artificial uninterrupted discontinuity) and particularly experiment B (artificial interrupted discontinuity). Model dimensions for the indentations and the rock mass correspond to average dimensions of experimental specimens from Experiments C and B (see Filippi et al., 2018). The definitions of discontinuity geometries are presented below.

In the first experiment, the formation of arcades can be observed in the region of the manually predefined horizontal indentation in the sandstone. We assume that the indentation can be used to model a higher susceptibility of sandstone to erosion in this region. That is why we set higher critical stress values for the discontinuity when compared with the rock mass (Table 1). High stress is necessary to stabilize the material in discontinuity and protect it from erosion when compared with the surrounding rock. For modeling purposes, we consider the upper part of the sandstone massif above the incision as well as the incision itself. We simulated the

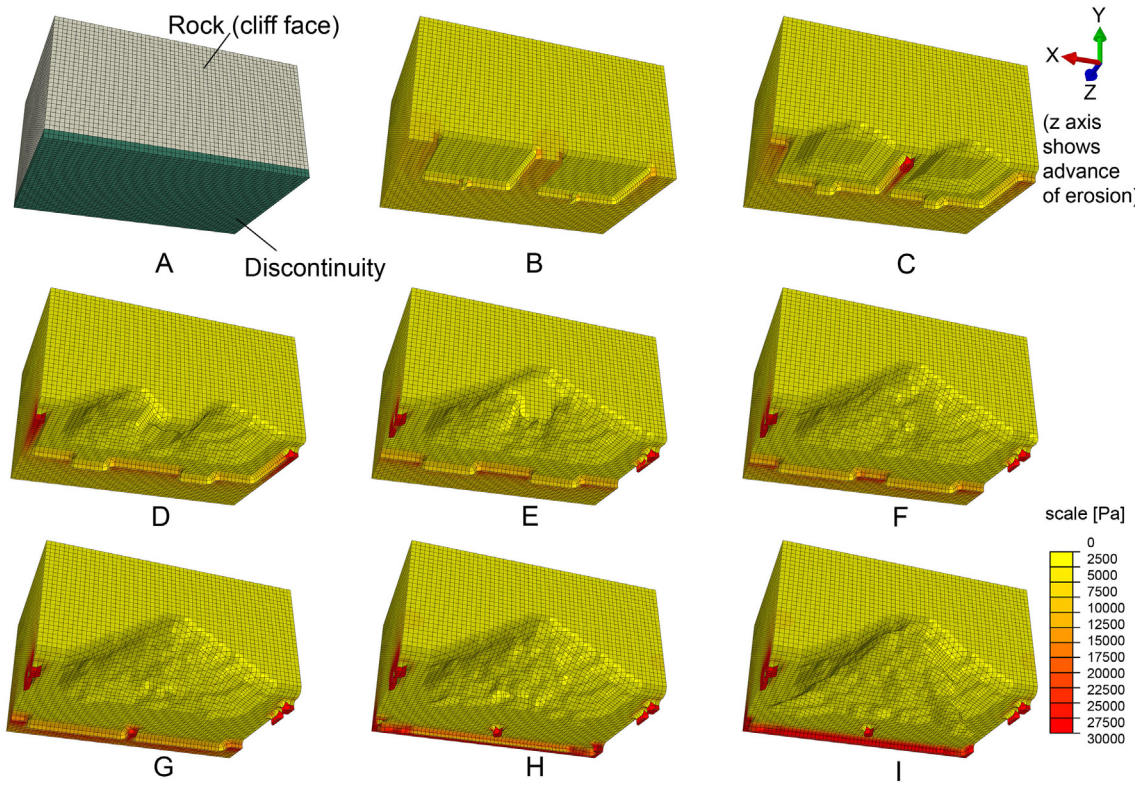


Fig. 3. Modeling of the erosion process with several indentations in a rock. A: Geometrical model including the discontinuity region and regular rock. Dimensions and boundary conditions are described in the Methods section. Panels B–I: Progress of the erosion process in relation to the iteration step, n . Non-eroded part of the model is shown together with the distribution of maximum stresses. All stresses in the discontinuity region exceeding the material disintegration limit are shown as disintegration limit stresses. B: Non-eroded part of the model at $n = 1$. Two initially eroded zones, 100 mm deep and 105 mm wide, can be seen in the discontinuity region, corresponding to indentations made during the experiment. Indentations are located symmetrically about the central section of the model, with a 30-mm non-eroded space separating them. To model the presence of discontinuities we added the eroded zone in the discontinuity region in the form of 20 mm deep and 4 mm wide stripes adjacent to the middle of indentations boundary. C: $n = 3$. Formation of arcades above the initial indentations. D: $n = 5$, E: $n = 8$, F: $n = 11$. Erosion of the region between the indentations and elimination of the central pillar. Merging of two smaller arcades into a single large one. Advance of the erosion front and widening of the additional indentation. Formation of the first row of pillars at sides of the model. G: $n = 14$, H: $n = 17$. Formation of the next row of pillars resulting from the advance of the erosion front. I: $n = 35$. The ultimate shape of a large arcade.

advance of the erosion front by expansion of the indentation and formation of pillars (Fig. 2 and Video 1 in Supplementary information). In the second experiment, we modeled the evolution of arcades during the sandstone erosion at the presence of several predefined

horizontal indentations. We observed behaviors such as the merging of two smaller arcades into a single large one and the formation of several rows of pillars resulting from the advance of the erosion front (Fig. 3 and Video 2 in Supplementary information).

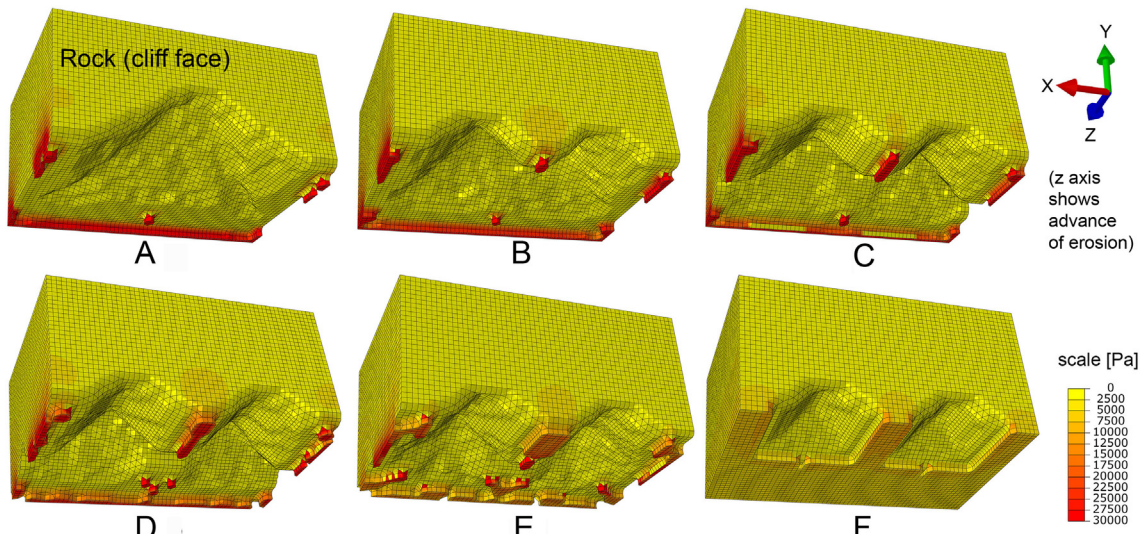


Fig. 4. The model of experiment B with different critical values set for the discontinuity zone. Panels A–F: Final structures formed at the end of the erosion process. The critical value for sandstone is kept constant. A: $\sigma_{CD} = 3.0 \cdot 10^4$ Pa. B: $\sigma_{CD} = 2.5 \cdot 10^4$ Pa. C: $\sigma_{CD} = 2.0 \cdot 10^4$ Pa. D: $\sigma_{CD} = 1.5 \cdot 10^4$ Pa. E: $\sigma_{CD} = 1.0 \cdot 10^4$ Pa. F: $\sigma_{CD} = 2.0 \cdot 10^2$ Pa.

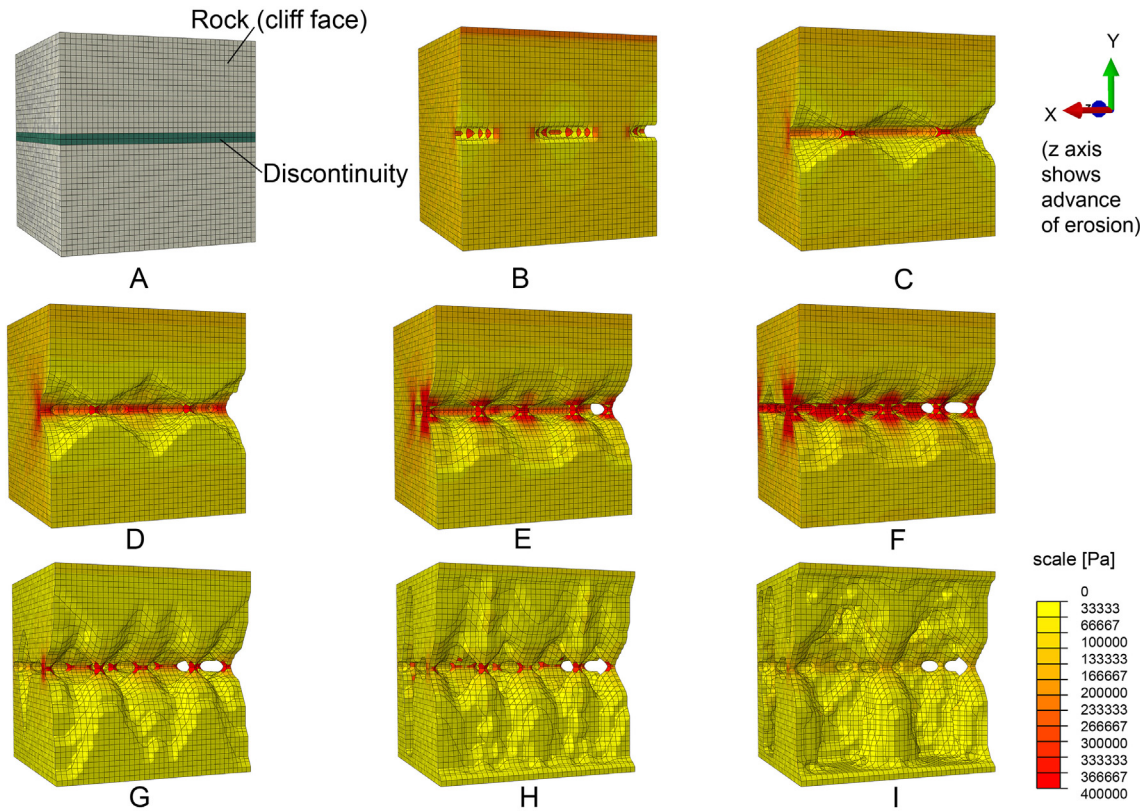


Fig. 5. Modeling the formation of various arcade types and pillars. A: Geometrical model including the discontinuity region and regular rock. See the Methods section for a description of model dimensions and boundary conditions. Panels B–F: Progress of the erosion process in relation to the iteration step, n , during modeling. Non-eroded part of the model is shown, together with the distribution of maximum stresses. All stresses in the discontinuity region exceeding the material disintegration limit are shown as disintegration limit stresses. B: Non-eroded model at $n = 1$. Three eroded zones are added to the discontinuity region in the form of circles with a radius of 30 mm and with their centers located at the free faces. C: $n = 4$. Formation of lenticular arcades. D: $n = 6$. Formation of the first two pillars near the free face. E: $n = 14$. Formation of additional pillars in the first row of pillars. F: $n = 45$. Propagation of the erosion front into the massif and formation of a second row of pillars when the erosion process becomes stationary. Formation of the complex 3D structure of rhombic arcades. Panels G–I: Modeling the erosion process at a subsequent decrease in the stress applied to the model. The evolution of rhombic arcades into hourglass-shaped pillars. G: $P = 27.5 \cdot 10^3 \text{ Pa}$. H: $P = 16.5 \cdot 10^3 \text{ Pa}$. I: $P = 11.0 \cdot 10^3 \text{ Pa}$.

We also performed modeling for experiment B with different critical stress values for the sandstone and horizontal indentation zones. We found that a reduction in the critical value for the horizontal indentation zone results in an increase in the number and size of pillars in the structure after erosion is completed with a corresponding reduction in the volume of eroded material (Fig. 4).

3.1.1. Modeling of experiment C (artificial uninterrupted indentation/discontinuity)

In the numerical model, we set the 50 mm deep initially eroded area within the discontinuity region, which corresponds to the indentation made in the experiment. To model the presence of discontinuities, we also added an eroded area in the form of a circle with a radius of 20 mm and its center located in the middle of the indentation boundary (Fig. 2B–I). To visualize the distribution of maximum stress, we set the limit for visualization equal to the material disintegration limit in the region of the discontinuity. This means that all stresses exceeding the critical stress will be depicted using one color corresponding to the critical stress. Such stresses keep the material stable, and it is thus not necessary to distinguish between them. Stresses below the critical stress, which enable erosion, are then better visible in numerical modeling outputs.

First, we can observe the advance of the erosion front and widening of an additional circular indentation (Fig. 2C, D). As this erosion occurs, the maximum stress area coincides with the corner area, where the linear front of erosion merges with the erosion front from the indentation. As the erosion front propagates, stress in the non-eroded zone of the discontinuity increases, and formation of the first row of pillars is observed in the corner area as the stresses in this area exceed the critical

stress (Fig. 2E, F). After the formation of the primary pillars is completed, the erosion front advances further, forming new pillars (Fig. 2G–I, Video 1 in Supplementary Information). Pillars thus emerge due to the local maxima of stress in the forefront of propagating erosion.

3.1.2. Modeling of experiment B (artificial interrupted indentation/discontinuity)

In the numerical model, we set two initially eroded zones 100 mm deep and 105 mm wide in the discontinuity region, corresponding to the predefined indentations made during the experiment. Two indentations are located symmetrically about the central section of the model, with 30 mm non-eroded space between them. The width of non-eroded zones at the sides of the model is 30 mm. To model the presence of discontinuities, we also added the eroded zone in the discontinuity region in the form of 20 mm deep and 5 mm wide stripes adjacent to the middle of the indentation boundary. The model at the first iteration step is shown in Fig. 3B. Further, Fig. 3C–I show the progress in the erosion process, depicting the non-eroded part of the model. First, the formation of arcades can be observed above the initial indentations (Fig. 3C), together with the formation of the central pillar. This is followed by the erosion of the area between indentations and elimination of the central pillar and by merging two smaller arcades into a single large one (Fig. 3D–F). The formation of the first row of pillars can be also observed at the sides of the model. The formation of another row of pillars comes next, resulting from the advance of the erosion front (Fig. 3G, H). The erosion process is completed with the development of the final shape of a large arcade (Fig. 3I, Video 2 in Supplementary information).

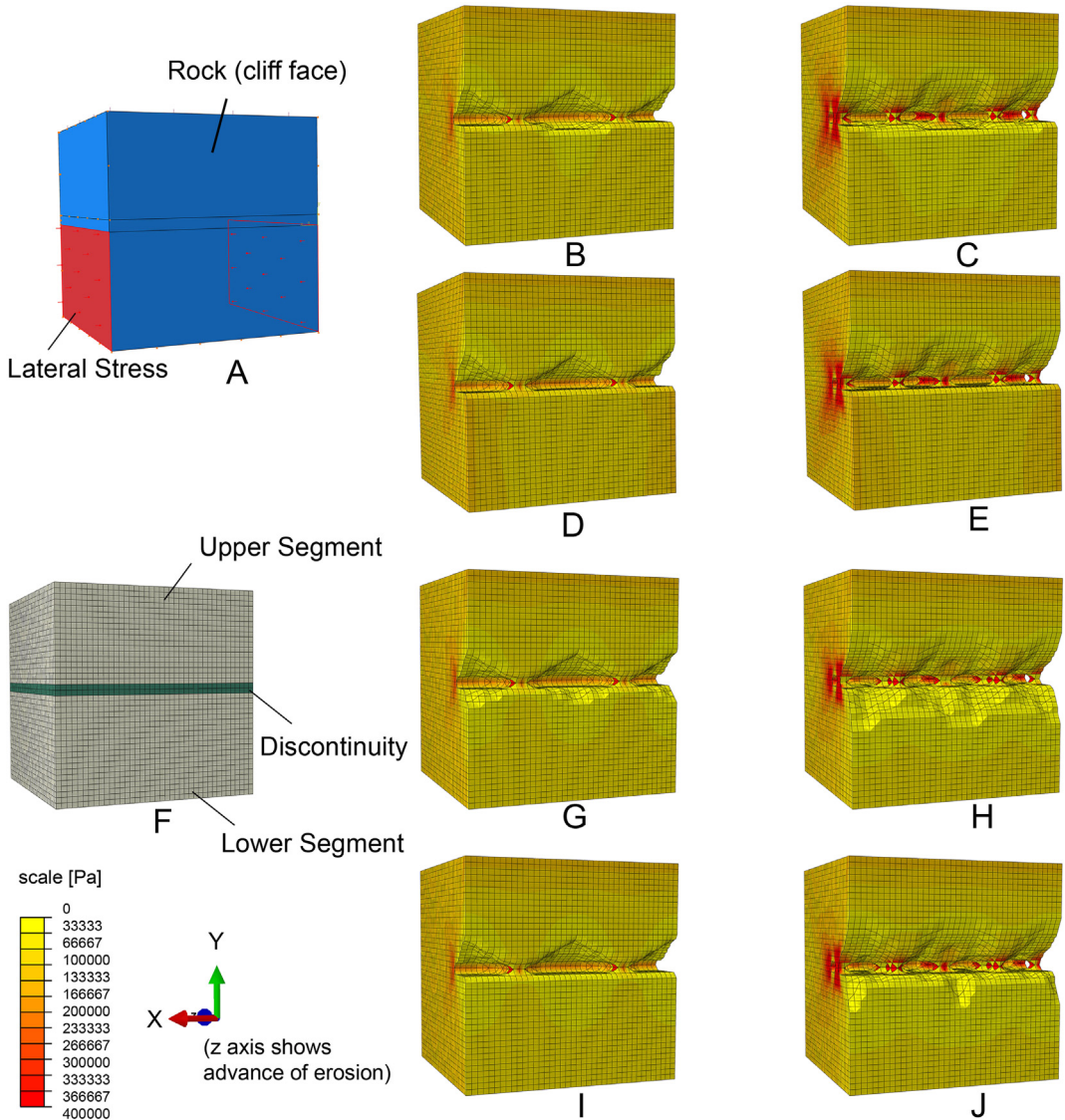


Fig. 6. Modeling the formation of asymmetrical arcades. Panels A–E: Presence of nonuniform distribution of lateral stresses. A: Geometrical model—pressure P_l is applied to the lower segment of side faces. B, C: $P_l = 5 \cdot 10^4 \text{ Pa}$. D, E: $P_l = 10^5 \text{ Pa}$. B, D: Formation of asymmetrical arcades. C, E: Formation of the first row of asymmetrical pillars. Panels F–J: nonuniform distribution of disintegration limit values. F: Geometrical model—various disintegration limit values are assigned for the lower segment of the model, σ_{cLower} . G, H: $\sigma_{cLower} = 4 \cdot 10^3 \text{ Pa}$. I, J: $\sigma_{cLower} = 2 \cdot 10^3 \text{ Pa}$. G, I: Formation of asymmetrical arcades. H, J: Formation of the first row of asymmetrical pillars.

3.1.3. Modeling of experiment B with various critical stress values

We considered the model used for experiment B (Fig. 3A) to analyze the impact of various critical stress values on modeling results. Results of the modeling of the arcade formation after the erosion process is completed are shown in Fig. 4 with various critical values for the discontinuity zone. The critical stress value for the sandstone was kept

constant. The following critical values were considered for the discontinuity zone: $\sigma_{cD} = 3.0 \cdot 10^4 \text{ Pa}$ (Fig. 4A) (initial value), $\sigma_{cD} = 2.5 \cdot 10^4 \text{ Pa}$ (Fig. 4B), $\sigma_{cD} = 2.0 \cdot 10^4 \text{ Pa}$ (Fig. 4C), $\sigma_{cD} = 1.5 \cdot 10^4 \text{ Pa}$ (Fig. 4D), $\sigma_{cD} = 1.0 \cdot 10^4 \text{ Pa}$ (Fig. 4E), and $\sigma_{cD} = 2.0 \cdot 10^2 \text{ Pa}$ (Fig. 4F). An increase in the number of pillars was observed with the reduction in the value of σ_{cD} . As this takes place, the area of pillar foundations also increases, as does the

Table 1
Properties of materials.

	Young's modulus			Poisson's ratio			Shear modulus			Critical value	
	$E_x (\text{Pa})$	$E_y (\text{Pa})$	$E_z (\text{Pa})$	ν_{yx}	ν_{xz}	ν_{yz}	$G_{yx} (\text{Pa})$	$G_{xz} (\text{Pa})$	$G_{yz} (\text{Pa})$	$\sigma_c (\text{Pa})$	
	Rock	Discontinuity									
Material 1 ^a (non-eroded)	$2 \cdot 10^7$	$2 \cdot 10^7$	$2 \cdot 10^7$	0.2	0.2	0.2	$8.3 \cdot 10^6$	$8.3 \cdot 10^6$	$8.3 \cdot 10^6$	$2 \cdot 10^2$	$3 \cdot 10^4$
Material 1 (eroded)	$2 \cdot 10^3$	$2 \cdot 10^3$	$2 \cdot 10^3$	0.2	0.2	0.2	$8.3 \cdot 10^2$	$8.3 \cdot 10^2$	$8.3 \cdot 10^2$	–	–
Material 2 (non-eroded)	$2 \cdot 10^7$	$2 \cdot 10^7$	$2 \cdot 10^7$	0.2	0.2	0.2	$8.3 \cdot 10^6$	$8.3 \cdot 10^6$	$8.3 \cdot 10^6$	$2 \cdot 10^4$	–
Material 2 (eroded)	$2 \cdot 10^3$	$2 \cdot 10^3$	$2 \cdot 10^3$	0.2	0.2	0.2	$8.3 \cdot 10^2$	$8.3 \cdot 10^2$	$8.3 \cdot 10^2$	–	–
Material 3 (non-eroded)	$2 \cdot 10^5$	$2 \cdot 10^7$	$2 \cdot 10^5$	0.2	0.2	0.2	$8.3 \cdot 10^4$	$8.3 \cdot 10^4$	$8.3 \cdot 10^4$	–	$4 \cdot 10^5$
Material 3 (eroded)	20	$2 \cdot 10^3$	20	0.2	0.2	0.2	8.3	8.3	8.3	–	–

^a For material characteristics, see the Methods section.

width of the pillars. Also, a decrease in the height of pillars and corresponding decreases in the height and volume of the eroded region were observed. When the critical value for the discontinuity zone was set equal to that for sandstone, $\sigma_{cs} = 2.0 \cdot 10^2 \text{ Pa}$ (Fig. 4F), no propagation of the erosion front into the discontinuity beyond the limits of initially eroded zones was observed, and only the formation of arcades over the initially eroded zones occurred.

3.2. New modeling without preformed horizontal indentations

Primarily, we modeled the formation of various arcade types observed in nature. A numerical model of the cubic shape was used. A discontinuity was located in the middle of the model, on the horizontal central cross section (Fig. 5A). Two different examples of arcades—symmetrical (lenticular) and asymmetrical (half-lenticular)—were modeled. In addition, the situation with two discontinuities located close to each other was modeled to observe the impact of the overlap of stress shadows. The particular examples are described below.

3.2.1. Modeling of symmetrical arcades and pillars

To model the presence of discontinuities, we added three circular eroded zones, 30 mm in radius, in the discontinuity region with their centers located at the free face. The center of one of the zones was located in the middle of the free face, and the centers of the other two were located at the intersection of side faces (Fig. 5B). Initially, the formation of arcades is observed during the advance of the erosion front (Fig. 5C). Then, the formation of the first two pillars is seen near the free face, where the erosion fronts propagating from initially eroded zones intersect (Fig. 5D). As the erosion front advances deeper into the model, additional pillars are formed in the first row of pillars (Fig. 5E). Then another two parallel rows of pillars are observed to form in the depth of the model. The formation of a complex 3D structure of rhombic arcades is also visible. We then lowered the stress applied to the model to represent the erosion of a part of the overburden, which resulted in the evolution of rhombic arcades into hourglass-shaped pillars (Fig. 5G–I, Video 3 in Supplementary information). At the end of this video, the primary pillars are narrowed and then destroyed, before arcades of higher order develop with massive pillars. These are forms (i.e., large arcades created by the merging of two or smaller arcade pits) often documented in nature.

3.2.2. Modeling of asymmetrical arcades

We analyzed two possible reasons for the development of asymmetrical arcades: the presence of nonuniform distribution of lateral stresses (Fig. 6A–E) and different critical stress values below and above discontinuity, which represents the common fact that discontinuity separates materials with more or less different mechanical properties (Fig. 6F–J). In the first case, instead of imposing lateral displacement constraints (along x -axis), we applied pressure P_L to the lower segment of the side faces (Fig. 6A). Calculations were conducted for two values of P_L , namely, $P_L = 5 \cdot 10^4 \text{ Pa}$ (Fig. 6B, C) and $P_L = 10^5 \text{ Pa}$ (Fig. 6D, E). Fig. 6B, D show the stages of the asymmetrical arcade formation, and Fig. 6C, E show various formation stages of the first row of asymmetrical pillars. For higher P_L values, no erosion takes place in the lower segment of the model (Fig. 6D, E). In the second case, we set various values for the critical stress disintegration limit for the lower segment of the model (Lower Segment) σ_{clower} (Fig. 6F). Calculations were performed for two values of σ_{clower} : $\sigma_{clower} = 4 \cdot 10^3 \text{ Pa}$ (Fig. 6G, H) and $\sigma_{clower} = 2 \cdot 10^3 \text{ Pa}$ (Fig. 6I, J). Fig. 6G, I show stages of the asymmetrical arcade formation, and Fig. 6H, J show the various formation stages of the first row of asymmetrical pillars. For lower values of σ_{clower} no erosion is visible in the lower segment of the model for the stage of asymmetrical arcade formation (Fig. 6I), and only a negligible erosion zone can be found in the lower segment of the model during the formation of asymmetrical pillars (Fig. 6J).

3.2.3. Modeling of a situation with two neighboring discontinuities

Finally, we modeled the formation of arcades and pillars on two neighboring discontinuities located symmetrically about the horizontal plane of symmetry (Fig. 7A). The distance between the discontinuities was one-third of the height of the model. Two situations were modeled: (i) parallel (Fig. 7B) and (ii) checkerboard arrangements of initial pits (Fig. 7C). Fig. 7D–I show the modeling results of arcade formation after the completion of the erosion process. Fig. 7D–F show results for the parallel arrangement of initial pits. Formation of large, complex-shaped vertical pillars tapering in the discontinuity regions and thickening in the area between the pillars was observed (Fig. 7D). Fig. 7E, F show the results for a modified model with removed fixing restraints for the back wall. The change in the boundary conditions has an insignificant impact on the erosion process initiation, i.e., on the formation of the first row of pillars. However, we found that in this case the erosion front propagation stops inside the model (see the side view in Fig. 7F), which differs significantly from the initial model, where the erosion front reaches the back wall (Fig. 7D). Fig. 7F also shows the formation of “tunnels” behind the first row of pillars. The formation of “tunnels” and the interruption of the erosion front propagation are related in that there are stress shadows formed around pillars in the discontinuity zone after the formation of the first row of pillars. When the erosion front moves within the stress shadow region, the shape of the front straightens and becomes more linear and parallel to the front side. With a continued propagation of the erosion front, an increase in the stress level can be observed in the non-eroded material behind the erosion front. When the front line becomes fully straightened and parallel to the front side (wall), the stress distribution within the non-eroded material behind the erosion front becomes uniform. Next, as the erosion front propagates further, stress increases until it exceeds the critical value over the whole erosion front at a certain moment, resulting in the cessation of erosion in the discontinuity region. In turn, the presence of a discontinuity in the erosion front results in a nonuniform stress distribution and, as a result, at a certain moment, the stress exceeds the critical value only in certain local regions of the erosion front, where erosion stops and pillars start to form. Thus, the next row of pillars is formed together with a “tunnel” between the individual rows of pillars.

Fig. 7G–I show the results for the checkerboard arrangement of initial pits. In Fig. 7G, the first row of pillars is formed in the discontinuity zones, also arranged in a checkerboard pattern. The formation of a zig-zag structure within the area of the first row of pillars is observed in the region between the discontinuities, because of being related to the direction of load paths between pillars in the discontinuity region. In both cases of boundary conditions imposed on the back side (see Fig. 7G for displacement restriction conditions and Fig. 7H, I where displacement restrictions are removed), propagation of the erosion front through the whole model, up to the back side, is observed. In addition, the formation of cavities inside the model is observed. This is because the structure obtained during the erosion process is a merger of pillars tapering in the zone of discontinuities and thickening outside this zone. Because the initial checkerboard pattern of pits is rather irregular, the erosion front propagates in a nonuniform manner and has no opportunity to straighten up, as is the case with the parallel arrangement of initial pits. This, in turn, results in an irregular arrangement of pillars and longer distances between adjacent pillars. Therefore, situations may occur where neighboring pillars do not intersect outside the discontinuity zone, thereby forming cavities (Fig. 7I).

4. Discussion

4.1. Real conditions versus modeling settings and limitations

Arcades represent a good example to study the origin of natural phenomena using the method of computational morphogenesis (Kelly, 1998; Age et al., 2017). However, previous models could not explain

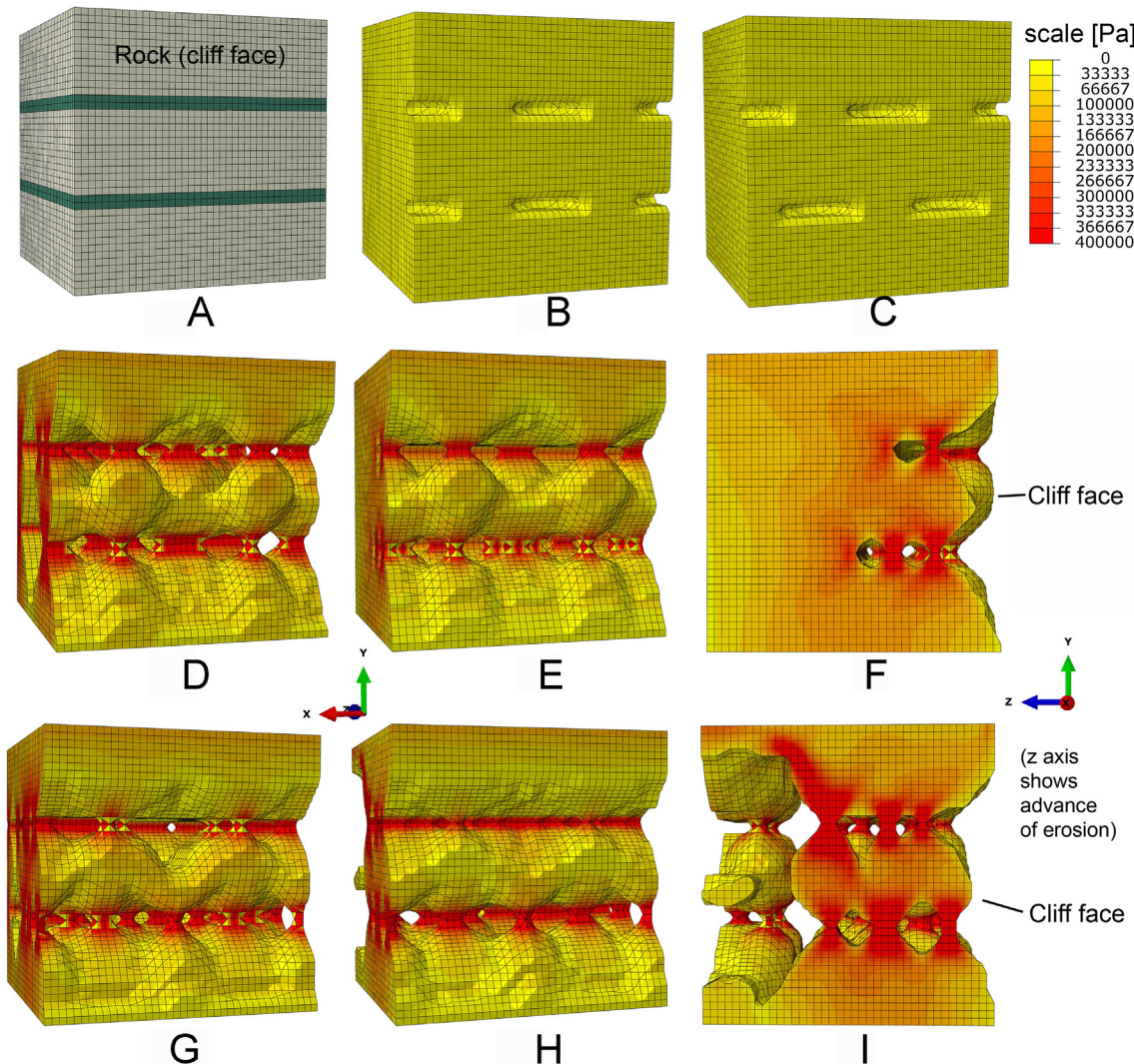


Fig. 7. Modeling the formation of arcades and pillars on two neighboring discontinuities. (modeling results after completion of the erosion process) A: Geometrical model. B: Parallel arrangement of initial pits. C: Checkerboard arrangement of initial pits. Panels D–F: Modeling results for the case of parallel arrangement of initial pits. D: Formation of large, complex-shaped vertical pillars tapering in discontinuity areas and thickening in the areas between discontinuities. E, F: Modeling results for a modified model with removed fixing restraints for the back wall. E: Front view. F: Side view. Termination of the erosion front propagation inside the model and formation of “tunnels”. Panels G–I: Modeling results for the case of checkerboard arrangement of initial pits. G: Formation of a zigzag structure inside the sandstone in the zone of the first row of pillars between the discontinuities. H, I: Modeling results for a modified model with removed fixing restraints for the back wall. H: Front view. I: Side view. Note the formation of cavities inside the model.

nances in arcade shapes and rather demonstrated the 3D arcade evolution in a qualitative way.

Various factors are considered to be essential for the development of “classical” weathering forms (honeycombs/tafoni), especially: temperature and climatic variations, presence/absence of salts, growth and destruction of surface biological and mineral crusts, and the extent of hydraulic field (McGreevy, 1982; Mottershead et al., 2003; Huinink et al., 2004; McBride and Picard, 2004; Rijniers et al., 2005; André and Hall, 2005; Mustoe, 2010; Adamović et al., 2011; Bruthans et al., 2018; Wieler et al., 2019). It would be difficult to include these factors in the modeling of arcade shapes. First, because their influence changes or ceases over time and space, and secondly, their exact role and importance in a detailed shaping of cavernous forms is actually unknown yet (Mottershead, 1994; Mol and Viles, 2012; Bruthans et al., 2018). Fortunately, as shown by the previous physical modeling (Filippi et al., 2018), it is not necessary to take these factors into account. It was documented that arcades of similar shapes occur in rocks of various lithologies, such as weak sandstones (or even locked sands), more cemented sandstones, quartzites, granites, and rhyolite tuffs (Filippi et al., 2018). It is also known that arcades of slightly different shapes and sizes can be observed in a small area, i.e., on a single discontinuity or several

adjacent discontinuities (e.g., Fig. 8A). In such a small volume of rock, no major variations in porosity, grain shape/size, and mineral composition/cementation can be presumed. In addition, arcades commonly form in rather homogeneous rocks composed of well-sorted materials, e.g., sand dunes or beach sands. All these observations point to a conclusion that most lithological features are not the controlling factors for shaping arcades and pillars. However, the character, frequency, inclination, and depth range of the discontinuities are demonstrably different at various sites. In other words, they differ in their distribution and the shapes of stress shadows. Principal stress directions are another factor that is difficult to consider in a model. Inclined axes of pillars or the asymmetry of some arcades and pillars prove that the rock stress principal directions are not always parallel to the gravity vector (Fig. 8B–E). Because the discontinuity geometry, stress intensity, and stress shadows geometry are difficult to measure in natural environment, numerical models are based on several theoretical examples. The individual examples represent simple cases, which often occur in nature. Erosion outcomes are significantly dependent on critical values for discontinuities and the rock, as well as on the rock-fixing conditions and distribution of lateral stresses, as was shown in the modeling results (Figs. 4, 6, 7). In modeling real objects, one should consider the internal

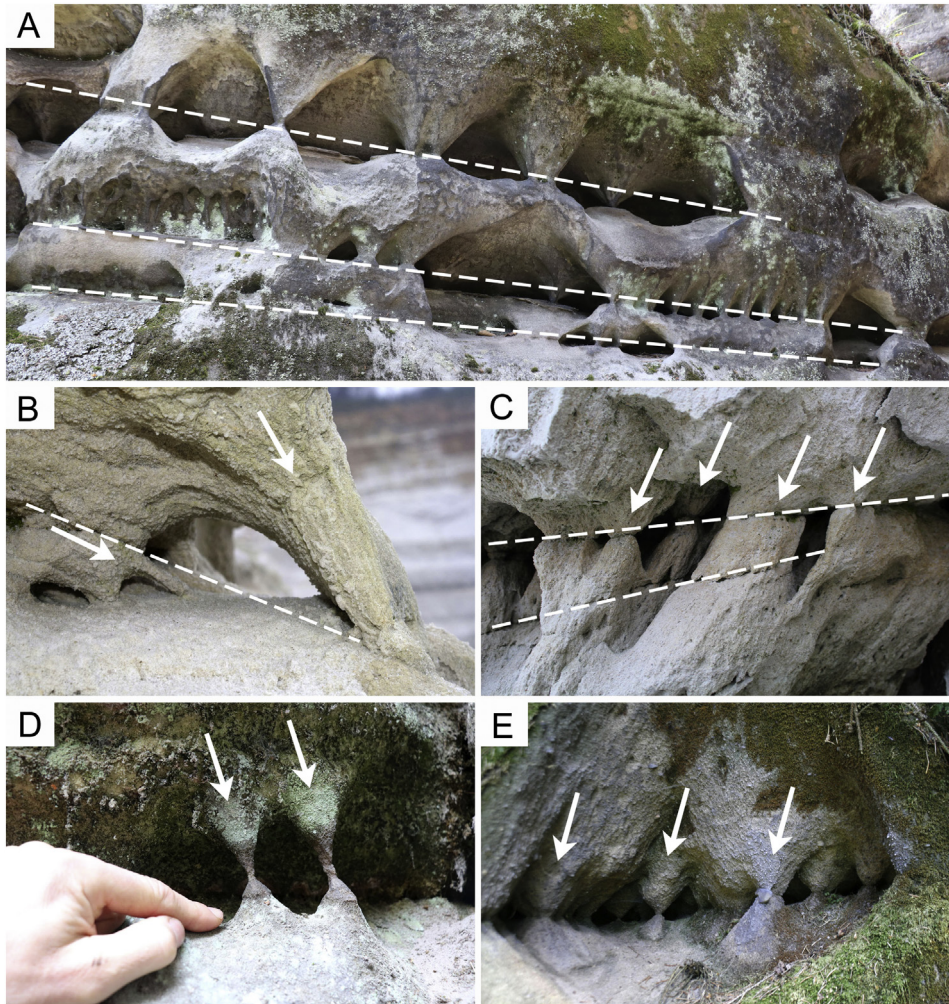


Fig. 8. Examples of arcades and pillars of various shapes, sizes, and inclinations. A: Various arcades on a small portion of the rock exposure, Apolena Rock City, CZ. B, C: Various young and still-developing inclined vaults and pillars in an artificial environment of the Střeleč Quarry, CZ. D: Old/stabilized (case-hardened and overgrown by lichens) inclined pillars exposed parallel to the surface, Apolena Rock City, CZ. E: Inclined pillars in an arcade cavity, Malobratice rock exposure, CZ. (arrows indicate stress directions; scale bar = 10 cm).

character of the discontinuities, which can have a significant impact on the distribution of lateral stresses and fixing conditions of the rock where erosion occurs. This is illustrated in Fig. 7, which shows that variations in the arrangement of initial pits and boundary conditions at the back wall may result in a termination of the erosion process inside the model and the formation of “tunnels”, or in the formation of an irregular structure of pillars with cavities among them. The presence of different shapes of pillars and cavities is evident in nature (Figs. 1, 8, 9). “Tunnels” are also natural forms and have been documented (e.g., fig. 26E, F in Filippi et al., 2018). This shows that most of the observed arcade-related forms can be explained with the use of relatively simple settings of the initial discontinuity geometry and material properties, with varied arrangement of initial pits and boundary conditions.

The frequency and character of the discontinuities are most likely the main factors driving the efficiency of erosion agents. Based on this assumption, we use the type of a simply defined rock (without other specific parameters) for modeling and focus mainly on the parameters of discontinuities and stress intensity to achieve principally valid modeling results. The knowledge of the character of the discontinuities should be significant for detailed modeling. However, discontinuities are particularly difficult to sample and study; hence, some *in situ* tests are needed to characterize them and collect more detailed inputs for modeling.

4.2. New knowledge related to development of arcades and related forms

We developed fully 3D numerical models of the stress-controlled erosion involving fresh rock and discontinuity to demonstrate the evolution of arcades. The discontinuity is characterized by higher critical stress to protect the rock from erosion (i.e., by higher susceptibility to erosion). It has been demonstrated that even the simplest geometry leads to the development of individual pillars (Fig. 2) and 3D arcades (Fig. 3) in the model material. Arcade shapes in the model material (Fig. 5) show a good resemblance with those in the nature. It is demonstrated that arcade evolution is closely associated with the contrasting disintegration behavior of the fresh rock mass and discontinuity. The models also demonstrate in what respect is the arcade shape modified by changes in the overburden stress (Fig. 5).

Although arcades and discontinuity-related overhangs, arches, and hourglass-shaped pillars might be treated as separate forms, they should rather be considered to be products of an interconnected array of forms and a single process. This process takes place at various scales and rates, and the resulting shape can be observed or conserved at various stages of evolution. As a result, seemingly diverse morphological forms can be seen in nature. Our modeling shows that shallow indentations on one side and clusters of cavities with pillars on the other side are different stages of a single process. A similar finding was observed

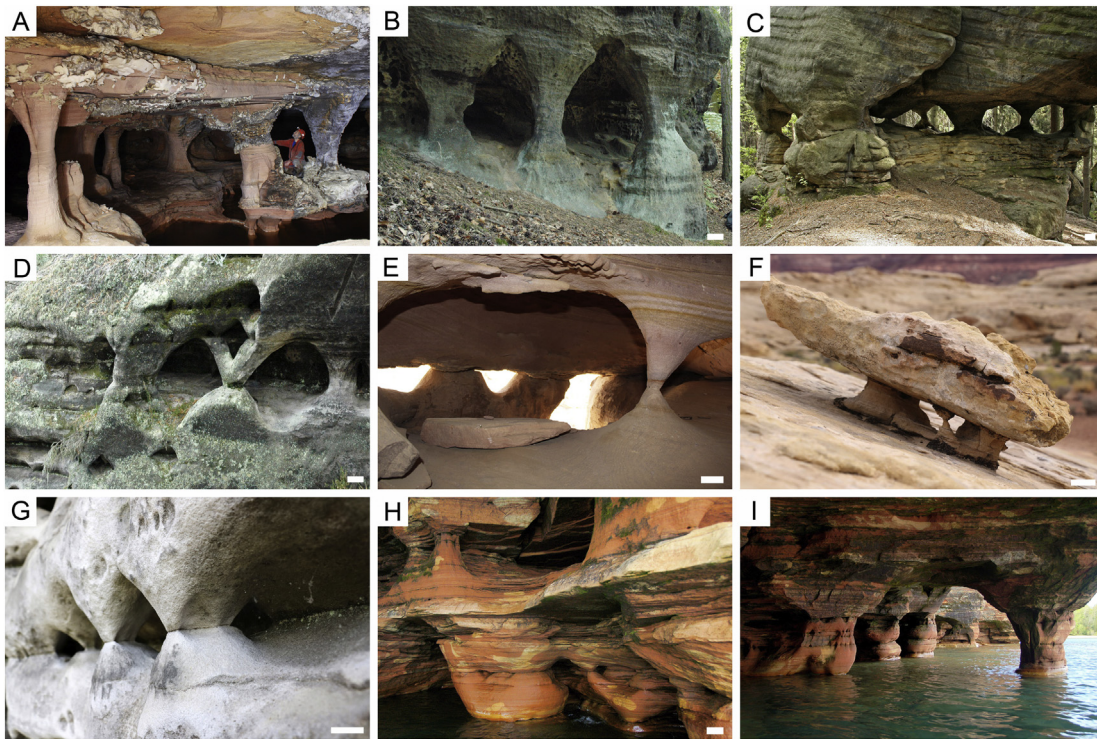


Fig. 9. Examples of different rock pillars (scale bar = 10 cm). A: An example of matured underground stream-derived roughly hourglass-shaped pillars (“3D distribution”) from Venezuelan quartz sandstone caves, Cueva Colibri Cave, Churí Tepui (photo by L. Láník). B: Large hourglass-shaped pillars on a cliff face (“2D distribution”), Kokořinský důl Valley, CZ. C: Hourglass-shaped pillars developed in a weaker layer (“3D distribution”) supporting a small rock tower, Svídnická Tower in the Adršpach-Teplice Cliffs monument, CZ (photo by O. Jenka). D: Arcades developed on neighboring discontinuities cause propagation of pillars at multiple levels one above another (note the V-shaped pillar), Apolena Rock City, CZ. E: Pillars developed on a single discontinuity—in a rock cavity (right) and on the cliff face (background), Petra area, Jordan. F: Pillars of different orientations developed in an inclined weathering sandstone layer beneath an indurated rock slab, Colorado River–Narrow Canyon, Utah, USA. G: Side view of a train of arcades on a cliff face showing the formation of a new arcade on the flank of the nearest pillar; this will later lead to splitting of this pillar into two smaller ones, Apolena Rock City, CZ. Examples B–G are salt crystallization-, freezing-, and precipitation-derived phenomena. H: Arcades and initial pillars developed on discontinuities of several levels. I: Large pillar and trains of small arcades. Examples H, I are lake level fluctuation- and freezing-derived phenomena, both Apostle Islands, Wisconsin, USA.

during the physical in situ modeling of an arch, where a narrow incision in a thin elongated rock body was found to be a sufficient precondition for the development of a perfect arch (Říhošek et al., 2019).

The presented models (Figs. 2–4) show some characteristic features, which have analogues in nature worldwide. The first experiment in this study resulted in the development of short pillars in a narrow incision, similar to those produced via physical experiments B and C with locked sands in Filippi et al. (2018) (figs. 18i and 19d therein) or those on natural outcrops (Fig. 1A, B). Our second experiment resulted in the merging of two neighboring arcades into a single larger one, which actually reflects the merging of two stress shadows. In other words, stress redistribution is caused by a change in the shape of the form, which, in turn, leads to its stabilization (Ostanin et al., 2017). The resulting form can be called an arcade of a “higher” order (cf. Figs. 3D–F and 5H, I with Fig. 1C, D).

Sharp-tipped (rhombic) shapes of arcade vaults are another characteristic feature connecting the results of our modeling with natural situations (cf. Figs. 3F and 5G with Fig. 1F–I). Sharp-tipped vaults appear not only in the early stages but also in the mature stages of our modeling. The common occurrence of rhombic and gently vaulted arcades at the same sites in outcrops confirms the hypothesis about a continuously evolving formational process where the shapes of arcades depend on the actual shapes of the stress shadows of evolving forms and on the cliff face geometry as a whole. Commonly, rhombic shapes are typical of soft rocks (portions of rocks) where rapid erosion does not provide sufficient time for stabilizing factors such as biologically initiated rock crust (Slavík et al., 2017; Wieler et al., 2019) or case hardening (Conca and Rossman, 1982) to become effective. Peaked/rhombic vaults are also seen on large-scale forms (Fig. 1G, H).

Various shapes of stress shadows during our modeling (see the yellow colored parts in the range 0–3333 Pa in Figs. 5–7; note both the frontal and inner parts of the forms) suggest that various areas are prone to erosion at various stages of the arcade evolution process. Considering that the formation of arcades is a long-term process, different erosion (or stabilization) factors may prevail at different stages/sites, and the development of the forms may be variable at each particular portion of a single outcrop (Figs. 1B, E, F, I, and 8A).

4.3. Implication for the origin of related landforms

We believe that numerical modeling could be helpful in the understanding of issues traditionally solved on the basis of lithological (mineralogical) controls, disregarding the effect of rock stress or other physical fields (cf. Huinink et al., 2004; Bruthans et al., 2018).

A good example is the controversy over the origin of pillars in the Venezuelan quartz sandstone caves (Fig. 9A), where two opposing hypotheses have been proposed: (i) selective induration of sandstone by descending fluids (“finger-flow theory”) (Aubrecht et al., 2011, 2013) and (ii) dissolution of quartz under structural and lithological control – pure “arenization theory” (Martini, 1979; Jennings, 1983; Sauro, 2014). Our modeling shows that the origin of pillars that are strikingly similar to those in Venezuela’s caves can be explained through erosion without any induration of the rock, as assumed by the finger-flow theory. In accordance with Sauro (2014), we would rather emphasize the importance of various sedimentary or tectonic discontinuities. Results of our modeling also clearly imply that spontaneous formation of rock pillars as by-products of the evolution of complex systems of arcade cavities should take place in various stress-controlled environments,

probably with contributions of various erosion agents/processes (Fig. 9B–I). Pillars in these photos, despite having a rather different appearance, share a common feature: the presence of nearly visible discontinuities of slightly varied orientations. We believe that these examples demonstrate that neither local cementation-induced induration nor quartz dissolution is needed as the primary cause for the shaping of the pillars. It is rather the 3D shape of the stress shadows along the preexisting discontinuities that allows the suite of erosion mechanisms to turn the stress shadows into hollows. The final shape of the pillars is then controlled by the resistance of various lithotypes to erosion, continuous redistribution of rock stress during the erosion process, and the availability of erosion agents and time for erosion to progress.

Symmetrical and asymmetrical arcades, as well as complex arcade structures with hourglass-shaped rock pillars, are certainly the main products of the stress-controlled and discontinuity related process. However, some other forms can be explained using this process, such as the pillars shown in Fig. 10A. These pillars with a slightly different appearance originate in a very young environment and probably cannot be straightforwardly associated with arcades only. Their origin is, however, controlled by the same principle, although with a contribution of small block collapses, derived by the presence of parallel vertical fractures and the undercutting (and material transport) provided by the underground stream. In addition to pillars, there are other related forms—rather protrusions from the ceiling or floors of cavities and caves—named “tetras” in Aubrecht et al. (2011) or “pendants” and “bumps” in Sauro (2014). We documented similar forms on the surface and consider them as relics of former pillars (Fig. 10B, C). They are, however, rather scarce; when a pillar is disrupted (and if not secondary indurated), its remaining parts, without support, are eroded rapidly (videos in Rihosek et al., 2016 and Filippi et al., 2018).

Besides caves in quartzose sandstones of Venezuelan Tepuis, there are other caves in the world where stress-controlled weathering appears to be a relevant factor at least for the initial stages of speleogenesis. The sandstone lake (“sea”) caves of the Apostle Islands in Lake Superior, Wisconsin, USA (c.f., Swanson, 2007), sandstone “phantom” (see below) cave Kaltbach in Switzerland (Häuselmann and Tognini, 2005), granitic caves of Sri Lanka (Osborn et al., 2013), and sandstone parts of the Sof Omar Cave System in southeastern Ethiopia (Asrat, 2015) can be mentioned as examples. All the characteristic features developed along discontinuities can be observed in these caves, such as arcades and 3D systems of large arched cavities with well-developed pillars.

4.4. Modeling results and relevant erosion processes

Arcades form due to the stress-controlled weathering/erosion along discontinuities and removal of loose materials. Observations on exposed faces of weak sandstone and locked sand in the Střeleč Quarry and physical experiments showed that arcades may evolve within minutes' time (Filippi et al., 2018). However, arcades occur also in solid rocks, even in quartzite or various granitic igneous rocks. In granitic rocks, disintegration is due to weathering along grain boundaries and decomposition/transformation of less stable minerals, which is followed by the transformation of a firm rocks into a saprolite (e.g., Begonha and Sequeira Braga, 2002; Riebe et al., 2017). Interestingly, the arcades were documented also in rocks and positions, which are far from the saprolite state (Filippi et al., 2018). It therefore seems probable that firm granular rocks can also be prone to stress-controlled erosion under some circumstances that are still not fully understood (cf., Noor-E-Khuda et al., 2017).

As has been recently demonstrated by laboratory experiments, various weathering processes are affected by stress, in particular salt and frost weathering, slaking, erosion by flowing water or rain drop impact (Bruthans et al., 2014, 2018; Rihosek et al., 2016). It is probable that other weathering processes are also affected by stress, although this has not been tested yet. Authors who dealt with discontinuity-related

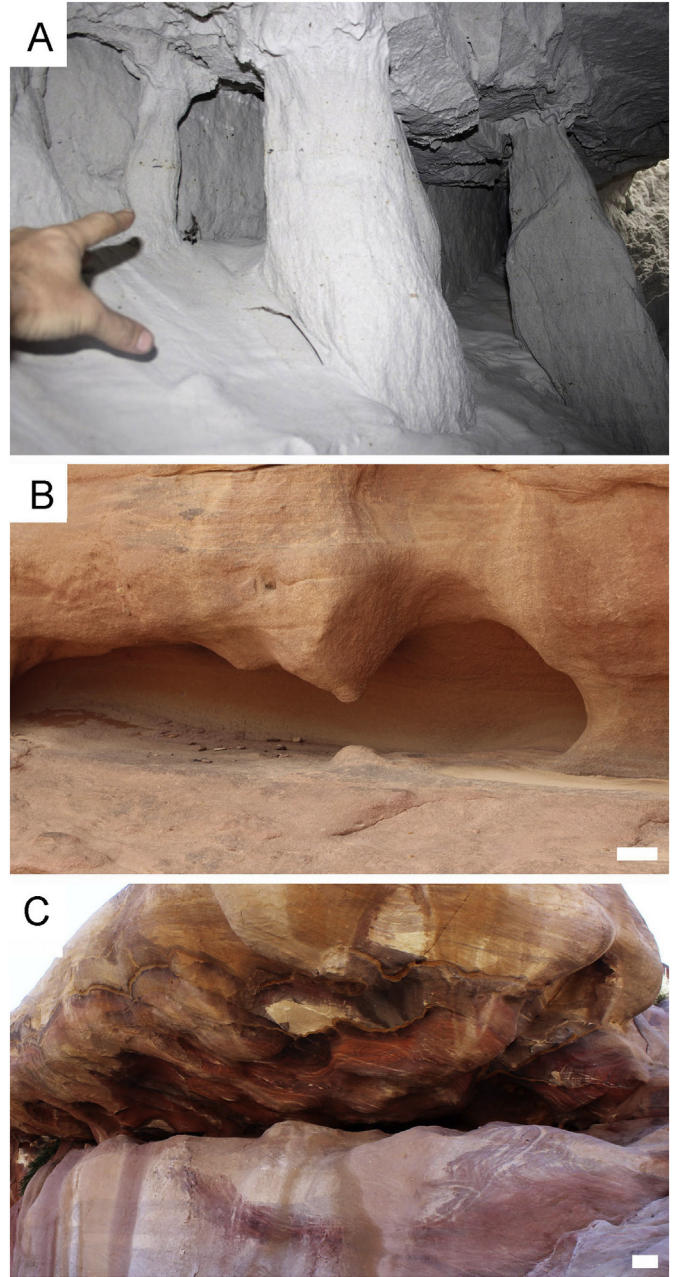


Fig. 10. Examples of specific rock pillars and pillar residues (scale bar = 10 cm). A: Pillars only several years old in an underground conduit developed along a zone of parallel vertical fractures in soft sandstone, Střeleč Quarry, CZ. B, C: Residues of pillars resembling tetras/pendants (Aubrecht et al., 2011; Sauro, 2014) in a cavity on a cliff face. Examples from Little Bridge area, Wadi Rum (B), and Petra area (C), both Jordan.

cavities (arcades) explained very simply the disintegration of sandstone along discontinuities via poor cementation (Oberlander, 1977), dissolution of natural cement (Wyckoff, 1999), or via an increased seepage at places where bedding planes intersect the cliff face (Alexandrowicz, 1970; Robinson, 2007). The common denominator of these explanations is that an increase in moisture decreases the strength of sandstone (Hawkins and McConnell, 1992; Vásárhelyi and Ván, 2006; Verstrynge et al., 2014). However, why the regular shapes form has remained unaddressed. Our modeling offers a simple answer to this question. Moisture from the discontinuity seeps to pores from more open spaces close to the discontinuity toward the smaller ones deeper and weakens the rock either via slaking (Arulanandan and Heinzen, 1977; Bruthans et al., 2014), hydric dilatation (Ruedrich et al., 2011; Columbu et al., 2014), or frost weathering (McGreevy, 1982). It is well known that

high moisture content increases the effect of frost weathering (Hallet, 1983; Hall, 1988). Therefore, the freezing–thawing actions are most probably the major erosion process in areas subject to cold periods (e.g., Nicholson and Nicholson, 2000; Bruthans et al., 2017, 2018). The removal of material follows the shapes of stress shadows shown in our models (see the bright yellow color in Figs. 5–7) and creates weathering forms very similar to those documented in natural rock outcrops. Frost weathering of porous rock is an intricate process (Nicholson and Nicholson, 2000; Ruedrich et al., 2011; Labus and Bochen, 2012). Variations in the pore size around discontinuities may cause an increase in the suction pressure (crysotension) when compared with the homogeneous rock, which causes remarkably stronger effect of freezing on a wet rock (Walder and Hallet, 1986; Williams and Smith, 1989; Hohmann, 1997). Pressure associated with cryosuction can reach significant values, up to approximately 20 MPa (Takashi et al., 1981). Such stresses can easily disintegrate not only weak sandstone but also firmer rocks. High moisture levels also explain the lack of precipitated salts in arcades compared with the classical cavernous weathering forms (honeycombs and tafoni), which in turn develop mainly owing to the crystallization of salts (Mustoe, 1982; Adamović et al., 2011; Bruthans et al., 2018).

The transformation of highly lithified sandstone or even quartzite into a significantly weaker rock or even loose sand, which could be easily eroded and transported away, is called “arenization” (Martini, 1979; Jennings, 1983). Conceptually, dissolution along quartz crystal boundaries through water advection increases the total porosity and makes the rock mechanically weaker. Later, Mecchia et al. (2014) with contribution of knowledge of other studies (Derjaguin and Churaev, 1986; Pettijohn et al., 1987) improved this concept by arguing that mass transport from significantly small pores is controlled by the diffusion of H_4SiO_4 molecules to the zone of flowing water with undersaturated water with respect to quartz (details in Wray and Sauro, 2017). A similar process of rock weakening, which is called “phantomization” and produces a “ghost”/“phantom” rock, was presented recently for granular rocks with soluble and insoluble components (Quinif et al., 2006; Laverty, 2012; Dubois et al., 2014). This two-stage concept assumes the chemical dissolution and removal of soluble species producing a residual “ghost-rock” inside the unaltered bedrock. Later, during a higher hydrodynamic energy environment stage, flowing water mechanically removes the undissolved particles and creates open spaces (Wray and Sauro, 2017). Both, the arenization and phantomization concepts are considered as slow processes responsible for the origin of arcades (cavities) in quartzite and other similar rocks in subsurface, where salt and frost weathering processes do not act: the former due to the absence of subzero temperatures and the latter due to a high humidity, thereby disabling the evaporation and concentration of solutions.

Most probably, slow arenization causes loosening of the rock in a certain “larger” zone along the discontinuity. After the material becomes friable, the principle of interlocking and negative feedback between stress and erosion, described by Bruthans et al. (2014), activates. As a result, stress shadows of certain shapes are created, and the erosion agents remove material from these shadows.

In our modeling approach, we considered homogeneous material with artificially imposed discontinuities. The real process is, indeed, more complex, as the initiation of arcade evolution is bound to natural small-scale heterogeneities. They cause certain rock zones to become less loaded than the other and this is where the arcade evolution starts, progressing until they are large enough to redistribute load to such degree that it restricts further erosion using stress-controlled erosion mechanism.

The proposed modeling technique can be extended to heterogeneous rock materials by introducing different values of rigidity and critical stress for different constituents. In addition to the herein discussed structures, formation of structures characteristic solely of heterogeneous rock materials can be described, such as the so-called “ribs” appearing at the surface and directed parallel to the maximum principal

stress direction. The authors have already made certain progress toward modeling of such structures, which will be described in future publications.

5. Conclusion

In our innovative modeling approach, the initiation of arcades, i.e., stress-controlled connections of the upper and lower blocks through the discontinuity, developed spontaneously, and arcades formed without artificial incisions. When changing parameters of the setting, the propagation of the erosion front along the discontinuity can be observed as well as the formation of arcades, pillars, and complex 3D arcade structures. The presence of planar discontinuities was the only condition needed for the emergence of stress shadows and thus the formation of arcades and related structures. The shape of the resulting arcades was affected by the critical disintegration stress, which represented different properties of the weaker material within the discontinuity zone than in the rock massif. Other factors leading to the evolution of the arcade asymmetry are lateral stress and different disintegration properties of rock massif above and below arcades. Such approach to modeling better simulates the natural process, thus providing stronger evidence for the formation mechanism of arcades.

The actual mechanisms of sandstone disintegration within the arcades and pillars formation need to be studied in the future. Based on current knowledge and our modeling, the presence of moisture along the discontinuity and frost weathering have been discussed and considered as the most probable erosion processes.

Our results confirmed that numerical modeling is a powerful tool for studying the process of stress-controlled erosion. We believe that this approach will be useful in studying the weathering of granular rocks. In addition, it should be helpful for studying discontinuity-related conduits in sandstone/quartzite and other granular rocks and the degradation of man-made sandstone monuments carved from a bare rock.

Supplementary data to this article can be found online at <https://doi.org/10.1016/j.geomorph.2020.107260>.

Declaration of competing interest

The authors declare that they have no known competing financial interests or personal relationships that could have appeared to influence the work reported in this paper.

Acknowledgments

This study was cofinanced by the Czech Science Foundation (No. 19-14082S) and conducted with the institutional support RVO67985831 of the Institute of Geology of the Czech Academy of Sciences (M.F.) and with the institutional support of the Center for Geosphere Dynamics (UNCE/SCI/006) (D.M.). The authors thank Lisa Mol and Francesco Sauro for their valuable comments and suggestions on the first draft of the manuscript and Jiří Adamović for providing some field photographs, valuable comments, and improving the language of the paper. The authors greatly appreciate the suggestions of Gregory A. Pope and an anonymous reviewer and the help of handling editor Achim A. Beylisch.

References

- Aage, N., Andreassen, E., Lazarov, B.S., Sigmund, O., 2017. Giga-voxel computational morphogenesis for structural design. *Nature* 550, 84–86.
- Abaqus Analysis User Manual, 2014. Version 6.14. Available at: <http://www.3ds.com/productsservices/>.
- Adamović, J., Mikuláš, R., Schweigstilová, J., Böhmová, V. 2011. Porosity changes induced by salt weathering of sandstones, Bohemian Cretaceous Basin, Czech Republic. *Acta Geodyn. Geomater.* 8, 1 (161), 29–45.
- Alexandrowicz, Z., 1970. *Skalki piaskowcowe w okolicy Ciężkowic nad Białą*. Ochr. Przyr. 35, 281–335 (In Polish).
- André, M.F., Hall, K., 2005. Honeycomb development on Alexander Island, glacial history of George VI sound and palaeoclimatic implications (two step cliffs/Mars Oasis, W. Antarctica). *Geomorphology* 65, 117–138.

- Arulanandan, K., Heinzen, R.T., 1977. Factors influencing erosion in dispersive clays and methods of identification. *Proceedings of Erosion and Solid Matter Transport in Inland Waters*. vol. 122. IAHS-AISH, Paris, pp. 75–81.
- Asrat, A., 2015. Geology, geomorphology, geodiversity and geoconservation of the Sof Omar Cave System, Southeastern Ethiopia. *J. Afr. Earth Sci.* 108, 47–63.
- Aubrecht, R., Lánczos, T., Gregor, M., Schlögl, J., Šmídá, B., Liščák, P., Brewer-Carías, Ch., Vlček, L., 2011. Sandstone caves on Venezuelan tepuis: return to pseudokarst? *Geomorphology* 132, 351–365.
- Aubrecht, R., Lánczos, T., Gregor, M., Schlögl, J., Šmídá, B., Liščák, P., Brewer-Carías, C., Vlček, L., 2013. Reply to the comment on "Sandstone caves on Venezuelan tepuis: return to pseudokarst?". *Geomorphology* 197, 197–202.
- Begonha, A., Sequeira Braga, M.A., 2002. Weathering of the Oporto granite: geotechnical and physical properties. *Catena* 49, 57–76.
- Bruthans, J., Soukup, J., Vaculíkova, J., Filippi, M., Schweigstillova, J., Mayo, A.L., Masin, D., Kletetschka, G., Rihosek, J., 2014. Sandstone landforms shaped by negative feedback between stress and erosion. *Nat. Geosci.* 7, 597–601.
- Bruthans, J., Filippi, M., Schweigstillová, J., Rihóšek, J., 2017. Quantitative study of a rapidly weathering sandstone overhang. *Earth Surf. Process. Landf.* 42 (5), 711–723. <https://doi.org/10.1002/esp.4016>.
- Bruthans, J., Filippi, M., Slavík, M., Svbodová, E., 2018. Origin of honeycombs: testing the hydraulic and case hardening hypotheses. *Geomorphology* 303, 68–83.
- Columbu, S., Giocanda, A., Lezzerini, M., Marchi, M., 2014. Hydric dilatation of ignimbritic stones used in the church of Santa Maria di Otti (Oscigiri, northern Sardinia, Italy). *Ital. J. Geosci.* 133 (1), 149–160.
- Conca, J.L., Rossman, G.R., 1982. Case hardening of sandstone. *Geology* 10, 520–523.
- Derjaguin, B., Churaev, N., 1986. Properties of water layers adjacent to interfaces. In: Croxton, C. (Ed.), *Fluid Interfacial Phenomena*. Wiley, New York, p. 748.
- Dubois, C., Quinif, Y., Baele, J.-M., Barriquand, L., Bini, A., Bruxelles, L., Dandurand, G., Havron, C., Kaufmann, O., Lans, B., Maire, R., Martin, J., Rodet, J., Rowberry, M.D., Tognini, P., Vergari, A., 2014. The process of ghost-rock karstification and its role in the formation of cave systems. *Earth Sci. Rev.* 131, 116–148.
- Filippi, M., Bruthans, J., Rihóšek, J., Slavík, M., Adamovič, J., Mašín, D., 2018. Arcades: products of stress-controlled and discontinuity-related weathering. *Earth-Sci. Rev.* 180, 159–184.
- Hall, K., 1988. A laboratory simulation of rock breakdown due to freeze-thaw in a maritime Antarctic environment. *Earth Surf. Process. Land.* 13, 369–382.
- Hallet, B., 1983. The breakdown of rock due to freezing: a theoretical model. Fourth International Conference on Permafrost, Final Proceedings, pp. 433–438.
- Häuselmann, P., Tognini, P., 2005. Kaltbach Cave (Siebenhengste, Switzerland): phantom of the sandstone? *Acta Carsol.* 34 (2), 383–395.
- Hawkins, A.B., McConnell, B.J., 1992. Sensitivity of sandstone strength and deformability to changes in moisture content. *Q. Eng. Geol.* 25, 115–130.
- Hohmann, M., 1997. Soil freezing – the concept of soil water potential. State of the art. *Cold Reg. Sci. Technol.* 25, 101–110.
- Huinink, H.P., Pel, L., Kopinga, K., 2004. Simulating the growth of tafoni. *Earth Surf. Process. Land.* 29, 1225–1233.
- Jennings, J.N., 1983. Sandstone pseudokarst or karst? In: Young, R.W., Nanson, G.C. (Eds.), *Aspects of Australian Sandstone Landscapes*. Australian and New Zealand Geomorphology Group Spec. Publication. 1. University of Wollongong, Wollongong, pp. 21–30.
- Kelly, K., 1998. The third culture. *Science* 279, 992–993.
- Klarbring, A., Torstenfelt, B., 2010. Dynamical systems and topology optimization. *Struct. Multidisc. Optim.* 42, 179–192.
- Labus, M., Bochen, J., 2012. Sandstone degradation: an experimental study of accelerated weathering. *Environ. Earth Sci.* 67, 2027–2042.
- Laverty, M., 2012. Preparing the ground – new mechanisms for karst and speleogenesis: "alteration", fantomisation and replacement. *Cave Karst Sci.* 39 (2), 72–76.
- Martini, J.E.J., 1979. Karst in Black Reef quartzite near Kaapsehoop, Eastern Transval. *Ann. S. Afr. Geol. Surv.* 13, 115–128.
- McBride, E.F., Picard, M.D., 2004. Origin of honeycombs and related weathering forms in Oligocene Macigno sandstone, Tuscan coast near Livorno, Italy. *Earth Surf. Process. Landf.* 29, 713–735.
- McGreevy, J.P., 1982. Frost and salt weathering: further experimental results. *Earth Surf. Process. Land.* 7, 475–488.
- Mecchia, M., Sauro, F., Piccini, L., De Waele, J., Sanna, L., Tisato, N., Lira, J., Vergara, F., 2014. Geochemistry of surface and subsurface waters in quartz sandstones: significance for the geomorphic evolution of tepui table mountains (Gran Sabana, Venezuela). *J. Hydrol.* 511, 117–138.
- Mol, L., Viles, H., 2012. The role of rock surface hardness and internal moisture in tafoni development in sandstone. *Earth Surf. Process. Land.* 37, 301–314.
- Moore, J.R., Geimer, P.R., Finnegan, R., Bodtker, J., 2020. Between a beam and catenary: Influence of geometry on gravitational stresses and stability of natural rock arches. *Geomorphology* 364. <https://doi.org/10.1016/j.geomorph.2020.107244>.
- Mottershead, D.N., 1994. Spatial variation in intensity of alveolar weathering of a sandstone structure in a coastal environment, Weston-Super-Mare, UK. In: Robinson, D.A., Williams, R.B.G. (Eds.), *Rock Weathering and Landform Evolution*. Wiley, Chichester, pp. 151–174.
- Mottershead, D.N., Gorbushina, A., Lucas, G., Wright, J., 2003. The influence of marine salts, aspect and microbes in the weathering of sandstone in two historic structures. *Build. Environ.* 38, 1193–1204.
- Mustoe, G.E., 1982. The origin of honeycomb weathering. *Geol. Soc. Am. Bull.* 93, 108–115.
- Mustoe, G.E., 2010. Biogenic origin of coastal honeycomb weathering. *Earth Surf. Process. Land.* 35, 424–434.
- Nicholson, D.T., Nicholson, F.H., 2000. Physical deterioration of sedimentary rocks subjected to experimental freeze-thaw weathering. *Earth Surf. Process. Land.* 25, 1295–1307.
- Noor-E-Khuda, S., Albermani, S., Veidt, M., 2017. Flexural strength of weathered granites: influence of freeze and thaw cycles. *Constr. Build. Mat.* 156, 891–901.
- Oberlander, T.M., 1977. Origin of segmented cliffs in massive sandstones of southeastern Utah. In: Doebring, D.O. (Ed.), *Geomorphology of Arid Regions*. Allen and Unwin, Boston, pp. 79–114.
- Osborn, R.A.L., Wel lange, W.S., Jayasingha, P., Dandenya, A.S., Algiriy, A.K.P., Pogson, R.E., 2013. Caves and karst-like features in Proterozoic gneiss and Cambrian granite, southern and central Sri Lanka: an introduction. *Acta Carsol.* 42 (1), 25–48.
- Ostanin, I., Safonov, A., Osledets, I., 2017. Natural erosion of sandstone as shape optimisation. *Scientific Reports* 7, 17301 author correction available at. <https://doi.org/10.1038/s41598-018-24100-z>.
- Pettijohn, F.J., Potter, P.E., Siever, R., 1987. *Sand and Sandstone*. Springer-Verlag, New York.
- Quinif, Y., Meon, H., Yans, Y., 2006. Nature and dating of karstic filling in the Hainaut Province (Belgium). Karstic, geodynamic and paleogeographic implications. *Geodin. Acta* 19 (2), 73–85.
- Riebe, C.S., Hahm, W.J., Brantley, S.L., 2017. Controls on deep critical zone architecture: a historical review and four testable hypotheses. *Earth Surf. Proc. Land.* 42, 128–156.
- Rihosek, J., Bruthans, J., Masin, D., Filippi, M., Carling, G.T., Schweigstillova, J., 2016. Gravity-induced stress as a factor reducing decay of sandstone monuments in Petra, Jordan. *J. Cult. Herit.* 19, 415–425.
- Rihóšek, J., Slavík, M., Bruthans, J., Filippi, M., 2019. Evolution of natural rock arches: a realistic small-scale experiment. *Geology* 47, 71–74.
- Rijniers, L.A., Huinink, H.P., Pel, L., Kopinga, K., 2005. Experimental evidence of crystallization pressure inside porous media. *Phys. Rev. Lett.* 94, 075503.
- Robinson, D.A., 2007. *Geomorphology of the inland sandstone cliffs of Southeast England*. In: Härtel, H., Čílek, V., Herben, T., Jakcson, A., Williams, R. (Eds.), *Sandstone Landscapes*. Academia, Prague, pp. 44–51.
- Ruedrich, J., Kirchner, D., Siegesmund, S., 2011. Physical weathering of building stones induced by freeze-thaw action: a laboratory long-term study. *Environ. Earth Sci.* 63, 1573–1586.
- Safonov, A.A., 2018. Computing via natural erosion of sandstone. *Int. J. Parallel, Emergent Distrib. Syst.* 33, 742–751.
- Safonov, A.A., 2019. 3D topology optimization of continuous fiber-reinforced structures via natural evolution method. *Compos. Struct.* 215, 289–297.
- Safonov, A.A., 2020. Abaqus user subroutines for numerical modelling of evolving arcades and rock pillars during natural erosion. https://github.com/AlexASafonov/Natural_Erosion.
- Sauro, F., 2014. Structural and lithological guidance on speleogenesis in quartz-sandstone: evidence of the arenisation process. *Geomorphology* 226, 106–123.
- Sigmund, O., Petersson, J., 1998. Numerical instabilities in topology optimization: a survey on procedures dealing with checkerboards, mesh-dependencies and local minima. *Struct. Opt.* 16, 68–75.
- Slavík, M., Bruthans, J., Filippi, M., Schweigstillová, J., Falteisek, L., Rihóšek, J., 2017. Biologically-initiated rock crust on sandstone: mechanical and hydraulic properties and resistance to erosion. *Geomorphology* 67, 211–227.
- Swanson, S.K., 2007. Lithostratigraphic controls on bedding-plane fractures and the potential for discrete groundwater flow through a siliciclastic sandstone aquifer, southern Wisconsin. *Sed. Geol.* 197, 65–78.
- Takashi, T., Ohrai, T., Yamamoto, H., Okamoto, J., 1981. Upper limit of heaving pressure derived by pore-water pressure measurements of partially frozen soil. *Eng. Geol.* 18, 245–257.
- Vásárhelyi, B., Ván, P., 2006. Influence of water content on the strength of rock. *Eng. Geol.* 84, 70–74.
- Verstrynghe, E., Adriaens, R.T., Elsen, J., Van Balen, K., 2014. Multi-scale analysis on the influence of moisture on the mechanical behavior of ferruginous sandstone. *Constr. Build. Mater.* 54, 78–90.
- Walder, J., Hallet, B., 1986. The physical basis of frost weathering: toward a more fundamental and unified perspective. *Arct. Alp. Res.* 18, 27–32.
- Wieler, N., Ginat, H., Gillor, O., Angel, R., 2019. The origin and role of biological rock crusts in rocky desert weathering. *Biogeosciences* 16, 1133–1145.
- Williams, P.J., Smith, M.W., 1989. *The Frozen Earth*. Cambridge University Press, Cambridge, p. 306.
- Wray, R.A.L., Sauro, F., 2017. An updated global review of solutional weathering processes and forms in quartz sandstones and quartzites. *Earth-Sci. Rev.* 171, 520–557.
- Wyckoff, J., 1999. The works of weather. In: Wyckoff, J. (Ed.), *Reading the Earth/Landforms in the Making*. Adastra West, Inc., Mahwah, pp. 21–63.